Bilayer B₈₀ Structure: High Stability and Experimental Support for Existence

Yi-Sha Chen,^a Jing-Jing Guo,^a Peng-Bo Liu,^a Hui-Yan Zhao,^{a,*} Jing Wang,^a and Ying Liu^{a,b,*}

^a Department of Physics and Hebei Advanced Thin Film Laboratory, Hebei Normal University, Shijiazhuang 050024, Hebei, China

^b National Key Laboratory for Materials Simulation and Design, Beijing 100083,

China

* Corresponding author. Department of Physics and Hebei Advanced Thin Film Laboratory, Hebei Normal University, Shijiazhuang 050024, Hebei, China.

*Email: hyzhao@hebtu.edu.cn; yliu@hebtu.edu.cn

KEYWORDS: Boron clusters, B_{80} fullerene, Bilayer structure, Thermodynamic stability, Aromaticity

ABSTRACT: The recent experimental characterization of B₈₀ via photoelectron spectroscopy stimulated renewed interest in exploring B₈₀ clusters. Here, a D_{3h}symmetric B₈₀ bilayer structure has been proposed using density functional theory calculations. Ab initio molecular dynamics simulations confirm that the bilayer structure maintain its structural integrity up to 1400 K, indicating superior thermodynamic stability compared to previously known B₈₀ configurations, including the B₈₀ buckyball and volleyball-like structures. Vibrational frequency analysis confirms its kinetic stability. Electronic structure calculations reveals a HOMO-LUMO gap of 0.72 eV and pronounced aromaticity, further supported by a nucleus-independent chemical shift (NICS(0)) value of -44.3 ppm in the interlayer B-B bonds. The simulated photoelectron spectrum of the B₈₀ bilayer reproduces key experimental features, with vertical detachment energies agreeing with experimental peaks within 0.04 eV. These findings support the potential existence of this bilayer configuration, and enrich the structural diversity of boron clusters, offering promising prospects for applications in nanoscale electronics.

INTRODUCTION

Boron, characterized by three valence electrons (2s²2p¹), exhibits electron deficiency that drives boron nanostructures to adopt multi-center two-electron bonds. Such bonding properties not only compensate for boron's electron shortage but also give rise to remarkable structural diversity in boron clusters. Extensive research has revealed diverse topological configurations of boron nanostructures, including quasi-planar,

tubular, cage, core-shell and bilayer configurations¹⁻⁵.

In 2007, Yakobson and co-workers proposed the B_{80} "fullerene", in which each hexagon of the C_{60} framework hosts an additional boron atom⁶. This discovery spurred the design of numerous boron nanostructures—stable α -boron sheets⁷⁻⁸, nanotubes⁷⁻⁹ and nanoribbons¹⁰—and inspired tuning of B_{80} 's properties via embedded species¹¹⁻¹⁶, metal functionalization¹⁷⁻¹⁸ and heteroatom substitution¹⁹. Subsequent researches, however, demonstrated that the B_{80} core-shell structure (incorporating an inner B_{12} icosahedron) is energetically preferred over the hollow fullerene²⁰⁻²¹. This evolution from hollow to core–shell architectures paralleled the transformation of small boron clusters into bulk-like motifs, with the B_{12} icosahedron emerging as a recurring building block in larger clusters such as B_{92}^{22} , B_{96}^{23} , B_{98-102}^{24} and $B_{111-114}^{25}$ structures.

Elucidating boron cluster geometries remains challenging because of their unconventional bonding. Combined photoelectron spectroscopy (PES) and first-principles calculations have mapped out a size-dependent progression from planar/quasi-planar (n = 3-38, 41-42) to cage-like (n = 39-40) structures^{3, 26-32}. The experimental observation of B₃₆- (borophene)³³⁻³⁵ and B₄₀- (borospherene)²⁶ confirmed the stability of these motifs. Recently, the discovery of the B₄₈ bilayer has revealed a novel structure composed of strong covalent bonds, capable of forming stable two-dimensional bilayer phases³⁶. B₄₈ bilayer demonstrated considerable stability, with photoelectron spectra providing evidence of the corresponding anionic structure³⁷. Furthermore, experimental synthesis of bilayer boron sheets on Ag and Cu surfaces has led to a new understanding of boron motifs³⁸⁻³⁹. Subsequent investigations by Zhao *et*

 $al.^{40}$ on B_n clusters (n=52-64) revealed the competition between bilayer and core-shell configurations, with the bilayer being more stable at n = 52, 54, 60, and 62, while the core-shell structure dominated for other cluster sizes. Significantly, subsequent investigations have revealed the emergence of B₆₃ bilayer configurations, with studies demonstrating that configurations featuring three interlayer B-B bonds were found energetically superior to those with four interlayer B-B bonds⁴¹. These groundbreaking developments have invigorated scientific exploration of boron nanomaterials.

More recently, Choi and co-workers reported the first PES characterization of B₈₀-, reigniting interest in B₈₀-based architectures⁴². Here, we propose a *D*_{3*h*}-symmetric B₈₀ bilayer, whose simulated PES spectrum reproduces the key experimental bands—namely the X, A, and B bands—observed by Choi *et al.* To gain a deeper understanding of the structural rules of boron clusters, we conduct a comprehensive analysis of this B₈₀ bilayer.

METHODS

The B₈₀ bilayer and selected isomers were fully optimized at both the PBE0/6-311+G(d)⁴³ and TPSSh/6-311+G(d)⁴⁴⁻⁴⁵ levels, employing Grimme's D3 dispersion correction with Becke-Johnson damping (D3-BJ)⁴⁶⁻⁴⁷, as implemented in the Gaussian 16 package⁴⁸. Vibrational frequency analyses at the PBE0/6-311+G(d) level confirmed that all optimized structures corresponded to true local minima on the potential energy surface, as evidenced by the absence of imaginary frequencies. To obtain more accurate relative energies, single-point energies were performed using the def2-TZVP basis set

at the SCS-MP2 and DLPNO-CCSD(T) levels of theory, employing the ORCA(6.0) software package⁴⁹.

Ab initio molecular dynamics (AIMD) simulations were conducted within the canonical (NVT) ensemble using DMol³ package, with a total time of 8 ps and a time step of 1 fs^{50} . The Nosé-Hoover thermostat⁵¹ was employed for temperature control, with Nosé Q ratio and Yoshida parameter set to 2 and 3, respectively⁵². The initial temperature was set to 800 K and was gradually increased until the structure collapse was observed.

Additionally, adaptive natural density partitioning (AdNDP)⁵³, nucleus-independent chemical shifts (NICS)⁵⁴ and photoelectron spectroscopy (PES) were achieved by PBE0/6-311+G* in Gaussian 16 package⁴⁸. To benchmark the reliability of our computational protocol, PES simulations were also carried out for the well-characterized C_s and D_{2d} B₄₀- structures²⁶, showing excellent agreement with reported experimental data (Figure S11). Visualization and data analyses were carried out using Multiwfn⁵⁵ and Visual Molecular Dynamics (VMD)⁵⁶ software.

RESULTS AND DISCUSSION

Structure and Stability of B_{80} Bilayer. After energy minimization, the B_{80} bilayer with D_{3h} symmetry was obtained. This configuration comprised two symmetrically equivalent quasi-planar layers interconnected through three interlayer B-B bonds, forming a structure reminiscent of a "Bilayer Cake", as depicted in Figure 1. The

average interlayer bond length of B_{80} bilayer was 1.715 Å, closely matching that of bilayer- α borophene synthesized on Ag(111) substrate (1.8 Å)⁵⁷, bilayer- α ⁺ borophene B_{22} (1.76 Å) and freestanding $v_{1/12}$ bilayer borophene (1.73 Å)³⁸⁻³⁹. This similarity reinforced the structural rationality of the B_{80} bilayer. Additionally, the B_{80} bilayer contained pentagonal pyramid B_6 and hexagonal pyramidal B_7 units, satisfying the "Aufbau principle"⁵⁸⁻⁵⁹.

In fact, the B_{80} bilayer structure was designed based on an isomer (Figure S1) of C_{60} fullerene. Specifically, the construction approach involved three key steps: (1) The substitution of all carbon atoms in C_{60} with boron atoms to form a B_{60} framework; (2) Insertion of boron atoms at the center positions of all 12 pentagonal rings in the B_{60} structure; (3) Targeted placement of additional boron atoms at the centers of 8 selected hexagonal rings. Subsequent energy minimization results revealed that the B_{80} bilayer with D_{3h} symmetry exhibited the relatively lower energy state among the studied systems, as shown in Figure S2.

To evaluate the stability hierarchy of the B₈₀ bilayer, we selected three representative B₈₀ isomers (buckyball⁶⁰, core-shell²⁰, and volleyball⁶¹ configurations) as reference systems. Through single-point energy calculations performed at different levels of theory (see Table S1), we conducted an analysis of their relative stability. Within the density functional theory (DFT) framework, three functionals (PBE, PBE0 and TPSSh) consistently predicted the following stability hierarchy: Core-shell $(C_1)^{20} >$ Bilayer $(D_{3h}) >$ Buckyball $(T_h)^{60} >$ Volleyball $(T_h)^{61}$, while B3LYP showed deviant behavior. Notably, at the more accurate SCS-MP2 and DLPNO-CCSD(T) theoretical levels, the

stability order remained conserved for core-shell (C_1) > bilayer (D_{3h}) configurations. Meanwhile, the buckyball (T_h) and volleyball (T_h) isomers had comparable energies, which were higher than those of core-shell and bilayer. This computational evidence strongly suggested that the core-shell (C_1) and bilayer (D_{3h}) configurations maintained distinct energy advantages over their spherical structures across multiple theoretical approaches.

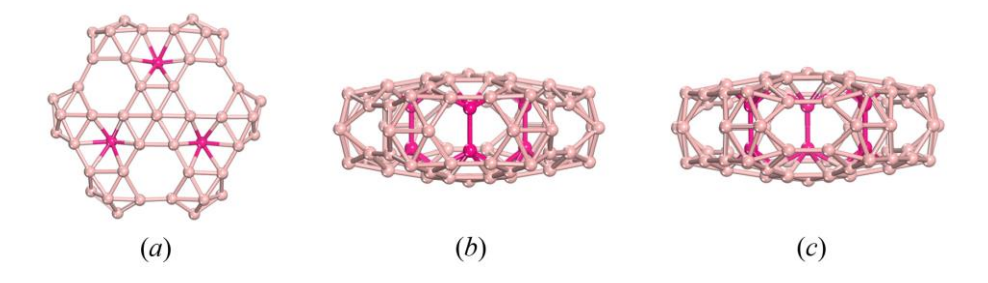


Figure 1. Top view (a), front view (b) and side view (c) of B₈₀ bilayer.

The Raman spectra of B₈₀ bilayer structure were performed, as shown in Figures S3. The results showed that the frequency of B₈₀ bilayer ranged from 141.1 cm⁻¹ to 1327.0 cm⁻¹. No imaginary frequencies were obtained, confirming that the B₈₀ bilayer structure was the local minima. Furthermore, the highest vibrational frequency of B₈₀ bilayer was 1003.0 cm⁻¹, corresponding to the vibration of the entire bilayer structure.

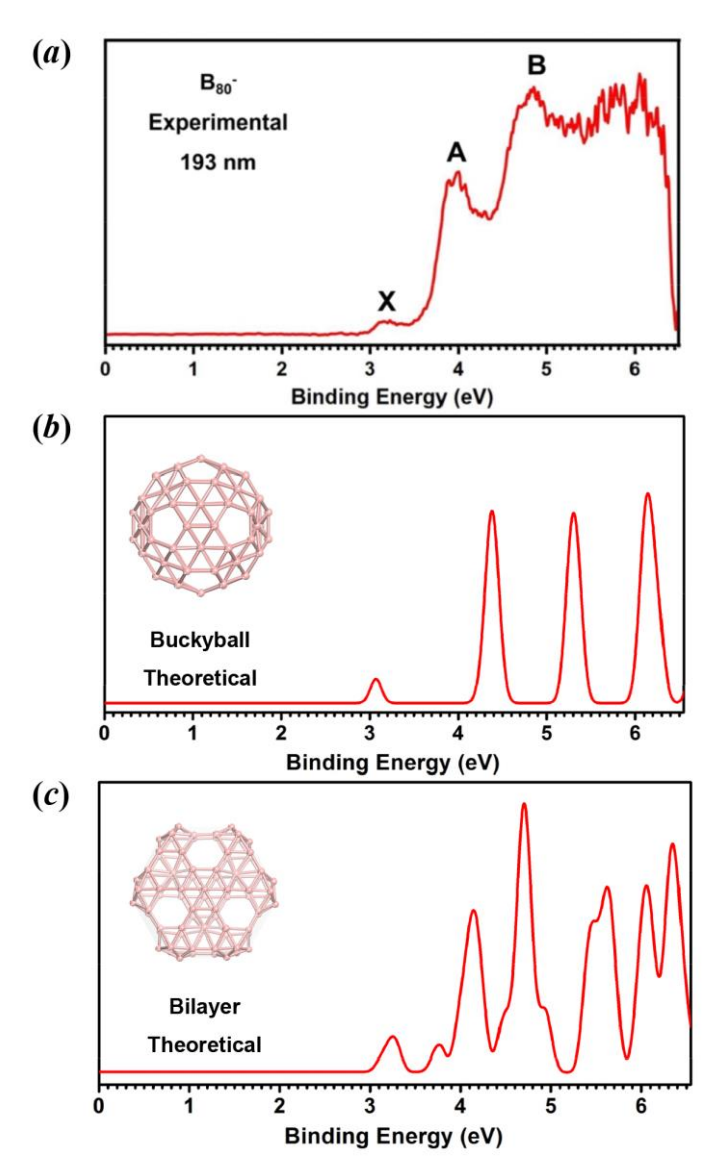


Figure 2. (a) Experimental photoelectron spectrum of B_{80}^- recorded at 193 nm (6.424 eV), adapted from Ref. 42. (b) Simulated photoelectron spectrum of the B_{80}^- buckyball at the PBE0 level. (c) Simulated photoelectron spectrum of the B_{80}^- bilayer at the PBE0 level.

Photoelectron spectroscopy, as powerful tools for probing gas-phase cluster structures, was employed to elucidate the structural and electronic properties of B_{80}^- bilayer and its isomers (Figure 2 and Figure S4). As shown in Figure 2 (*a*), Choi *et al*. clearly resolved three distinct PES bands (labeled as X, A and B) in the B_{80}^- , exhibiting

vertical detachment energies (VDEs) of 3.2 eV, 4.0 eV and 4.8 eV, respectively⁴². The spectral onset of band X provided an adiabatic detachment energy (ADE) of 3.1 eV. Theoretical simulations PES for the B₈₀- buckyball and B₈₀- bilayer structures, displayed in Figures 2 (*b*) and 2 (*c*), respectively, using Gaussian functions with a full width at half maximum of 0.15 eV. Both B₈₀- buckyball and B₈₀- bilayer structures well reproduced the major experimental spectral features (X, A and B). Besides, the B₈₀- buckyball configuration yielded ADE/VDE values of 3.09/3.10 eV at the PBE0 level, aligning with experimental X-band measurements (3.1/3.2 eV). Similarly, the B₈₀- bilayer structure showed calculated ADE/VDE values of 3.19/3.24 eV at the same theoretical level, closely matching the experimental X-band parameters. These results supported the possible existence of B₈₀- bilayer configurations.

AIMD simulations were performed to assess the thermodynamic stability of B_{80} clusters. The simulations were conducted using NVT ensemble, covering temperatures ranging from 800 K to 1600 K, as shown in Figure 3, Figures S5-S7. At 1400 K, it was observed that the B_{80} bilayer geometry can be well-kept and returned to its original structure after energy minimization, as depicted in Figure 3 (a). The average root-mean-square deviation (RMSD) of B_{80} bilayer at 1400 K was 0.29 Å, indicating that all atoms remained near their equilibrium positions (Figure S5). The AIMD final configuration of B_{80} core-shell structure at 1400 K showed characters of deformed the B_6 pentagonal or B_7 hexagonal pyramidal units, as well as the appearance of hollow octagon in the outer shell, while the B_{12} core remained intact, as shown in Figure 3 (b). Notably, although the B_{12} icosahedral core maintained structural integrity throughout the 8 ps

simulation trajectory, these morphological changes in the outer shell configuration compromised the overall structural stability. The hollow cage configurations of the B₈₀ fullerene and B₈₀ volleyball have been destroyed after 8 *ps* AIMD simulation. After energy minimization, neither the hollow cage structures of the B₈₀ fullerene and B₈₀ volleyball nor the B₈₀ core-shell structure could restore their initial configurations.

At 1500 K, after 8 ps AIMD simulation, the B₈₀ bilayer began to collapse, as shown in Figure S6 (a). The final configuration of B₈₀ core-shell structure has deformed and could not revert to its original structure after re-optimization. Interestingly, the B₁₂ icosahedron core in the B₈₀ core-shell structure was reconstructed by exchanging the inner and outer B atoms, as shown in Figure S6 (b). As the temperature increases, at 1600 K, B₈₀ core-shell structure completely collapsed, concurrent with the melting of the B₁₂ icosahedral core, as shown in Figure S7 (b). Computational analyses revealed a clear thermodynamic stability hierarchy among the investigated B₈₀ isomers, with the B₈₀ core-shell structure (1500 K) illustrated in Figure S6 (b) demonstrating the highest thermodynamic stability, followed sequentially by the B₈₀ bilayer (1400 K) shown in Figure 3 (a). The thermodynamic stability of the B₈₀ fullerene (about 1325 K) in Figure S7 (a) and B₈₀ volleyball (about 1325 K) in Figure S7 (a) were comparable.

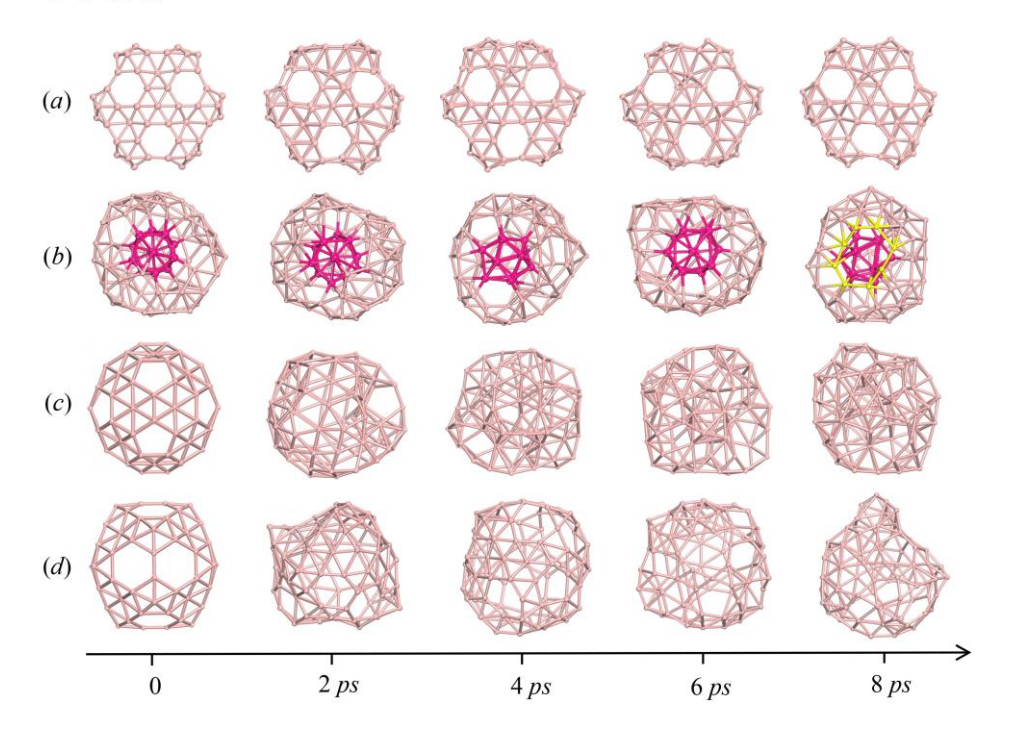


Figure 3. AIMD of the D_{3h} B₈₀ bilayer (a), C_1 B₈₀ core-shell structure (b), T_h B₈₀ fullerene (c) and T_h B₈₀ volleyball (d) at 1400 K; insets depicting snapshots at 0 ps, 2 ps, 4 ps, 6 ps, and 8 ps, with a total simulation time of 8 ps and a time step of 1 fs.

Electronic Structure of B₈₀ Bilayer. To investigate the electronic properties of B₈₀ bilayer structure, the electron density was calculated, as depicted in Figure 4, where regions of electron dissipation and accumulation were colored in yellow and blue, respectively. Figure 4 (a) revealed pronounced charge dissipation on the boron atoms at the center of the hexagon, accompanied by significant charge accumulation on the boron atoms at the edges of the hexagon. This distribution suggested that charge transfer occurred from the central boron atoms to the peripheral boron atoms. Figure 4 (b) demonstrated significant electron density localization in B₃ triangular configurations of the pentagonal pyramidal units and interlayer bridging B-B bonds.

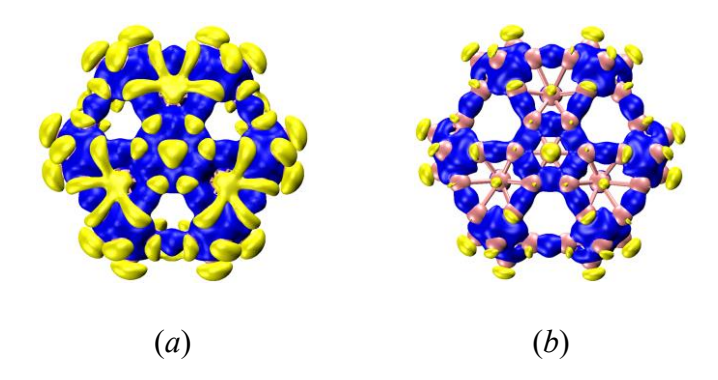


Figure 4. Deformation electron density of B_{80} bilayer, with the isosurfaces of 0.007 e/Å³ (a) and 0.015 e/Å³ (b). The blue and yellow regions represented electron accumulation and dissipation, respectively.

To further investigate the electronic properties of B_{80} bilayer structure, partial density of states (PDOS) and molecular frontier orbitals were analyzed, with the corresponding results shown in Figure 5 and Figure S8. The electronic structure analysis revealed a HOMO-LUMO gap of 0.72 eV, (indicated by purple and black dashed lines for HOMO and LUMO, respectively), demonstrating its good chemical inertness. Additionally, the PDOS indicated that the molecular orbitals of the B_{80} bilayer originated from hybridization of B 2s and B 2p orbitals, with significant contributions from the 2p orbitals, which was also evident in the HOMO and LUMO molecular orbitals shown in Figure S8.

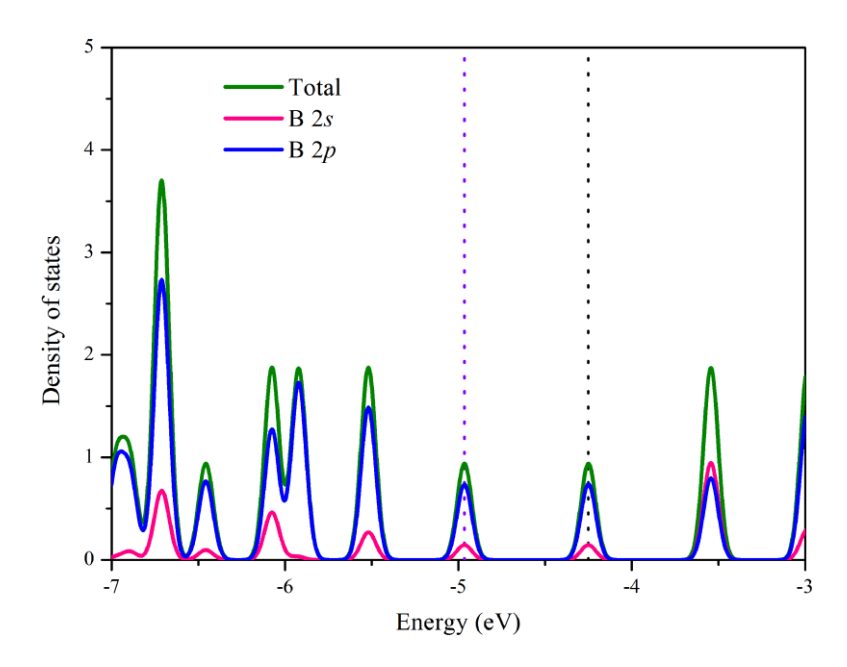


Figure 5. The total and partial density of states of B₈₀ bilayer. The HOMO (purple) and LUMO (black) levels were shown by dashed lines.

Furthermore, a detailed adaptive natural density partition (AdNDP) bonding analysis of B_{80} bilayer was performed, as shown in Figure 6. The 120 multi-center two-electron σ bonds found in the B_{80} bilayer played a crucial role in maintaining the stability of the B_{80} bilayer structure. Specifically, of all the 27 local 2c-2e σ bonds, 3 2c-2e σ bonds were located between the three interlayer B-B bonds, the remaining 24 2c-2e σ bonds were located at the hexagons of both the upper and lower layers. Two distinct types of 48 3c-2e σ bonds were found on the pentagonal pyramids at twelve corners of the bilayer structure. The remaining two types of 3c-2e σ bonds existed in the centered hexagons (B₇ units) of the structure. Delocalized 12 4c-2e σ bonds were located in the hexagonal pyramids and 6 delocalized 4c-2e σ bonds were located in the B₄ rhombi at the waist. Two types of 6c-2e σ bonds were situated in two different types of B₆ units at the waist. Furthermore, 9 10c-2e σ bonds connected the upper and lower layers of

the bilayer structure. These multi-center two-electron σ bonds were in agreement with the deformation electron density observed in the B_{80} bilayer.

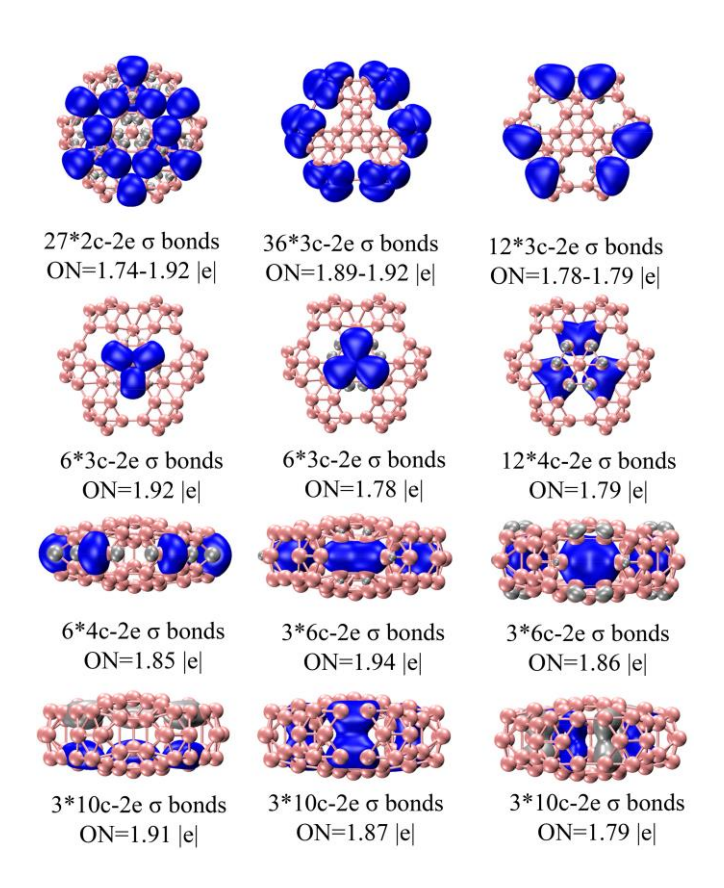


Figure 6. AdNDP for B₈₀ bilayer, with the occupation numbers (ONs) indicated.

To investigate the aromaticity of the B_{80} bilayer, we calculated the NICS-scanned curves in two different directions, as shown in Figure 7. The results revealed that the B_{80} bilayer exhibited aromatic characteristics. The NICS-scanned curves of B_{80} bilayer along the y-axis and z-axis confirmed that the bilayer structure was the aromatic system, with particularly strong aromaticity in the interlayer B-B bonds, which showed a NICS value of approximately -44.3 ppm in Figure 7 (a). The NICS value at the central region of the upper and lower layers was about -8.3 ppm in Figure 7 (b). The NICS scan along

the y-axis showed two peaks at ± 5 Å with positive NICS values, corresponding to the deshielded region localized in the waist of the bilayer structure, which are self-consistent with the ICSS-ZZ results (Iso-chemical shielding surface (ICSS) based on the calculated NICS-ZZ components), as illustrated in Figures S9 and S10. Additionally, the NICS scan along the z-axis displayed symmetry, with a NICS value of approximately -64.1 ppm at the center of the B atoms in the centered hexagon. The regions approximately 0.9 Å above and below the centered hexagon exhibited anti-aromatic characteristics, as indicated by positive NICS values. The remaining regions with negative NICS values represented shielding areas, further confirming that the bilayer structure possessed aromatic properties.

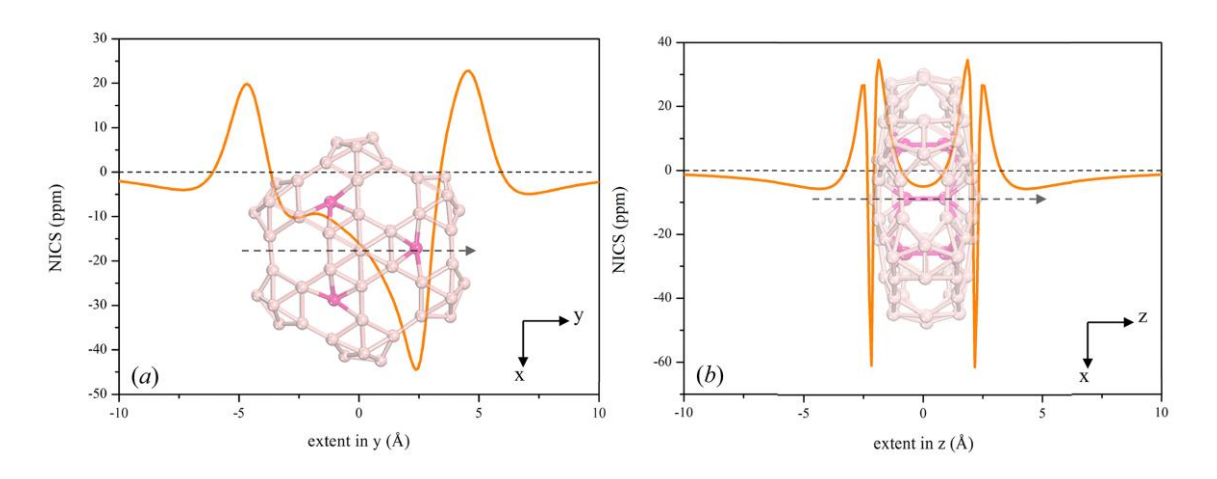


Figure 7. NICS-scanned curves on the y-axis (a) and the z-axis (b) of B₈₀ bilayer, respectively.

CONCLUSIONS

In summary, the B_{80} bilayer has been performed using the first principles calculation. The computational results suggested that the average interlayer bond length of B_{80}

bilayer was very close to that of bilayer borophene, further corroborating the structural rationality of B_{80} bilayer. Vibrational frequency analysis revealed that the B_{80} bilayer structure exhibits characteristic frequencies spanning 141.1 to 1327.0 cm⁻¹, with the absence of imaginary frequencies confirming the true local minimum on the potential energy surface. AIMD simulations demonstrated the following thermal stability hierarchy: B_{80} core-shell structure (1500 K) > B_{80} bilayer (1400 K) > B_{80} fullerene (about 1325 K) \approx B_{80} volleyball (about 1325 K). NICS-scanned curves analysis revealed pronounced aromatic characteristics, particularly at interlayer B-B bonding regions where the particularly strong aromaticity was observed (NICS = -44.1 ppm). Furthermore, the simulated photoelectron spectroscopy of the B_{80} bilayer exhibited significant alignment with experimental data, providing support for the potential existence of this bilayer structure. It is hoped that our work will contribute to a deeper understanding of B_{80} nanostructures.

ASSOCIATED CONTENT

Supporting Information

The Supporting Information is available free of charge.

Front view and side view of C_{60} structure; The optimized B_{80} isomers; Raman spectrum for the B_{80} bilayer; PES of the B_{80}^- volleyball and B_{80}^- core-shell structure; The details of RMSD of B_{80} bilayer; The results of AIMD simulations of the B_{80} clusters at different temperatures; Molecular frontier orbitals for the B_{80} bilayer; ICSS_ZZ of B_{80} bilayer; PES of the quasi-planar C_8 B_{40}^- and cage-like D_{2d} B_{40}^- ; The relative energies at different

levels of theory (PDF).

AUTHOR INFORMATION

Corresponding Authors

Ying Liu - Department of Physics and Hebei Advanced Thin Film Laboratory, National Key Laboratory for Materials Simulation and Design, Hebei Normal University, Shijiazhuang 050024, Hebei, China; Beijing 100083, China; orcid.org/0000-0002-7164-962X; Email: yliu@hebtu.edu.cn

Hui-Yan Zhao - Department of Physics and Hebei Advanced Thin Film Laboratory,

Hebei Normal University, Shijiazhuang 050024, Hebei, China; orcid.org/0000-0001
8548-9906; Email: hyzhao@hebtu.edu.cn

Authors

Yi-Sha Chen - Department of Physics and Hebei Advanced Thin Film Laboratory, Hebei Normal University, Shijiazhuang 050024, Hebei, China

Jing-Jing Guo - Department of Physics and Hebei Advanced Thin Film Laboratory, Hebei Normal University, Shijiazhuang 050024, Hebei, China

Peng-Bo Liu - Department of Physics and Hebei Advanced Thin Film Laboratory, Hebei Normal University, Shijiazhuang 050024, Hebei, China

Jing Wang - Department of Physics and Hebei Advanced Thin Film Laboratory, Hebei Normal University, Shijiazhuang 050024, Hebei, China

Author Contributions

Conceptualization, Hui-Yan Zhao and Ying Liu; Writing-original draft, Yi-Sha

Chen; Writing-review & editing, Yi-Sha Chen, Jing-Jing Guo, Peng-Bo Liu, Hui-Yan Zhao, Jing Wang; Validation, Hui-Yan Zhao and Ying Liu; Investigation, Hui-Yan Zhao and Ying Liu; Methodology, Yi-Sha Chen, Hui-Yan Zhao and Ying Liu; Funding acquisition, Yi-Sha Chen, Jing-Jing Guo, Peng-Bo Liu and Ying Liu.

Notes

The authors declare no competing financial interest.

ACKNOWLEDGMENTS

This work is granted by the National Natural Science Foundation of China (Grant Nos. 12174084 and 12404338), the Doctoral Research Start-up Foundation of Hebei Normal University (Grant Nos. L2023B08 and L2025B12), and the Innovation Funding Project for Doctoral Students of Hebei Province (Grant No. CXZZBS2025144).

REFERENCES

- (1) Sergeeva, A. P.; Popov, I. A.; Piazza, Z. A.; Li, W. L.; Romanescu, C.; Wang, L. S.; Boldyrev, A. I. Understanding Boron through Size-Selected Clusters: Structure, Chemical Bonding, and Fluxionality. *Acc. Chem. Res.* **2014**, *47* (4), 1349-1358.
- (2) Wang, L. S. Photoelectron Spectroscopy of Size-Selected Boron Clusters: From Planar Structures to Borophenes and Borospherenes. *Int. Rev. Phys. Chem.* **2016**, *35* (1), 69-142.
- (3) Jian, T.; Chen, X. N.; Li, S. D.; Boldyrev, A. I.; Li, J.; Wang, L. S. Probing the

- Structures and Bonding of Size-Selected Boron and Doped-Boron Clusters. *Chem. Soc. Rev.* **2019**, *48* (13), 3550-3591.
- (4) Barroso, J.; Pan, S.; Merino, G. Structural Transformations in Boron Clusters Induced by Metal Doping. *Chem. Soc. Rev.* **2022**, *51* (3), 1098-1123.
- (5) Chen, B.; He, K. H.; Dai, W.; Gutsev, G. L.; Lu, C. Geometric and Electronic Diversity of Metal Doped Boron Clusters. *J. Phys. Condens. Matter.* **2023**, *35* (18), 183002.
- (6) Gonzalez Szwacki, N.; Sadrzadeh, A.; Yakobson, B. I. B₈₀ Fullerene: An *Ab Initio* Prediction of Geometry, Stability, and Electronic Structure. *Phys. Rev. Lett.* 2007, 98 (16), 166804-166804.
- (7) Tang, H.; Ismail Beigi, S. Novel Precursors for Boron Nanotubes: The Competition of Two-Center and Three-Center Bonding in Boron Sheets. *Phys. Rev. Lett.* **2007**, *99* (11), 115501.
- (8) Yang, X. B.; Ding, Y.; Ni, J. *Ab Initio* Prediction of Stable Boron Sheets and Boron Nanotubes: Structure, Stability, and Electronic Properties. *Phys. Rev. B* **2008**, *77* (4), 041402.
- (9) Singh, A. K.; Sadrzadeh, A.; Yakobson, B. I. Probing Properties of Boron A-Tubes by *Ab Initio* Calculations. *Nano Lett.* **2008**, *8* (5), 1314-1317.
- (10) Ding, Y.; Yang, X. B.; Ni, J. Electronic Structures of Boron Nanoribbons. *Appl. Phys. Lett.* **2008**, *93* (4), 043107.
- (11) Wang, J. T.; Chen, C. F.; Wang, E. G.; Wang, D. S.; Mizuseki, H.; Kawazoe, Y. Highly Stable and Symmetric Boron Caged B@Co₁₂@B₈₀ Core-Shell Cluster. *Appl.*

- Phys. Lett. 2009, 94 (13), 133012.
- (12) Jin, P.; Hao, C.; Gao, Z. X.; Zhang, S. B.; Chen, Z. F. Endohedral Metalloborofullerenes La2@B₈₀ and Sc₃N@B₈₀: A Density Functional Theory Prediction. *J. Phys. Chem. A* **2009**, *113* (43), 11613-11618.
- (13) Liu, C.; Yang, L.; Jin, P.; Hou, Q. H.; Li, L. L. Computational Prediction of Endohedral Dimetalloborofullerenes M₂@B₈₀ (M = Sc, Y). *Chem. Phys. Lett.* **2017**, 676, 89-94.
- (14) Mahdavifar, Z.; Ershadifar, M.; Farrokhnia, A. Electro-Optical Properties and Structural Stability Perspectives of M₃N and M₂C₂ (M = Sc, La) Clusters Encapsulated in B₈₀ Fullerene: A Density Functional Theory Study. *J. Electron. Mater.* **2018**, *47* (1), 550-565.
- (15) Li, J. L.; Yang, G. W. Ni@B₈₀: A Single Molecular Magnetic Switch. *Appl. Phys. Lett.* **2009**, *95* (13), 133115.
- (16) Jin, P.; Liu, C.; Hou, Q. H.; Li, L. L.; Tang, C. C.; Chen, Z. F. Scandium Carbides/Cyanides in the Boron Cage: Computational Prediction of X@B₈₀ (X = Sc₂C₂, Sc₃C₂, Sc₃CN and Sc₃C₂CN). *Phys. Chem. Chem. Phys.* **2016**, *18* (31), 21398-21411.
- (17) Li, Y. C.; Zhou, G.; Li, J.; Gu, B. L.; Duan, W. H. Alkali-Metal-Doped B₈₀ as High-Capacity Hydrogen Storage Media. *J. Phys. Chem. C* **2008**, *112* (49), 19268-19271.
- (18) Li, J. L.; Hu, Z. S.; Yang, G. W. High-Capacity Hydrogen Storage of Magnesium-Decorated Boron Fullerene. *Chem. Phys.* **2012**, *392* (1), 16-20.
- (19) Li, F. Y.; Jiang, D. E.; Chen, Z. F. Computational Quest for Spherical C₁₂B₆₈ Fullerenes with "Magici" Π-Electrons and Quasi-Planar Tetra-Coordinated Carbon. J.

- Mol. Model. 2014, 20 (2), 2085.
- (20) Zhao, J. J.; Wang, L.; Li, F. Y.; Chen, Z. F. B₈₀ and Other Medium-Sized Boron Clusters: Core Shell Structures, Not Hollow Cages. *J. Phys. Chem. A* **2010**, *114* (37), 9969-9972.
- (21) Li, H.; Shao, N.; Shang, B.; Yuan, L. F.; Yang, J. L.; Zeng, X. C. Icosahedral B₁₂-Containing Core-Shell Structures of B₈₀. *Chem. Commun.* **2010**, *46* (22), 3878-3880.
- (22) Chen, Y. S.; Guo, J. J.; Liu, P. B.; Zhao, H. Y.; Wang, J.; Liu, Y. B₉₂: A Complete Coating Icosahedral B₁₂ Core–Shell Structure. *Phys. Chem. Chem. Phys.* **2025**, *27* (2), 655-659.
- (23) Sai, L. W.; Wu, X.; Li, F. Y. B₉₆: A Complete Core–Shell Structure with High Symmetry. *Phys. Chem. Chem. Phys.* **2022**, *24* (26), 15687-15690.
- (24) Prasad, D. L. V. K.; Jemmis, E. D. Stuffing Improves the Stability of Fullerenelike Boron Clusters. *Phys. Rev. Lett.* **2008**, *100* (16), 165504.
- (25) Zhang, M.; Lu, H. G.; Li, S. D. B₁₁₁, B₁₁₂, B₁₁₃, and B₁₁₄: The Most Stable Core-Shell Borospherenes with an Icosahedral B₁₂ Core at the Center Exhibiting Superatomic Behaviors. *Nano Res.* **2021**, *14* (12), 4719-4724.
- (26) Zhai, H. J.; Zhao, Y. F.; Li, W. L.; Chen, Q.; Bai, H.; Hu, H. S.; Piazza, Z. A.; Tian,
 W. J.; Lu, H. G.; Wu, Y. B.; Mu, Y. W.; Wei, G. F.; Liu, Z. P.; Li, J.; Li, S. D.; Wang, L.
 S. Observation of an All-Boron Fullerene. *Nat. Chem.* 2014, 6 (8), 727-731.
- (27) Sergeeva, A. P.; Zubarev, D. Y.; Zhai, H. J.; Boldyrev, A. I.; Wang, L. S. Photoelectron Spectroscopic and Theoretical Study of B₁₆⁻ and B₁₆²-: An All-Boron Naphthalene. *J. Am. Chem. Soc.* **2008**, *130* (23), 7244-7246.

- (28) Zhai, H. J.; Alexandrova, A. N.; Birch, K. A.; Boldyrev, A. I.; Wang, L. S. Hepta-and Octacoordinate Boron in Molecular Wheels of Eight- and Nine-Atom Boron Clusters: Observation and Confirmation. *Angew. Chem. Int. Edit.* **2003**, *42* (48), 6004-6008.
- (29) Huang, W.; Sergeeva, A. P.; Zhai, H. J.; Averkiev, B. B.; Wang, L. S.; Boldyrev, A. I. A Concentric Planar Doubly Π-Aromatic B₁₉- Cluster. *Nat. Chem.* **2010**, *2* (3), 202-206.
- (30) Chen, Q.; Chen, T. T.; Li, H. R.; Zhao, X. Y.; Chen, W. J.; Zhai, H. J.; Li, S. D.; Wang, L. S. B₃₁⁻ and B₃₂⁻: Chiral Quasi-Planar Boron Clusters. *Nanoscale* **2019**, *11* (19), 9698-9704.
- (31) Bai, H.; Chen, T. T.; Chen, Q.; Zhao, X. Y.; Zhang, Y. Y.; Chen, W. J.; Li, W. L.; Cheung, L. F.; Bai, B.; Cavanagh, J.; Huang, W.; Li, S. D.; Li, J.; Wang, L. S. Planar B₄₁⁻ and B₄₂⁻ Clusters with Double-Hexagonal Vacancies. *Nanoscale* **2019**, *11* (48), 23286-23295.
- (32) Chen, Q.; Li, W. L.; Zhao, Y. F.; Zhang, S. Y.; Hu, H. S.; Bai, H.; Li, H. R.; Tian, W. J.; Lu, H. G.; Zhai, H. J.; Li, S. D.; Li, J.; Wang, L. S. Experimental and Theoretical Evidence of an Axially Chiral Borospherene. *Acs Nano* **2015**, *9* (1), 754-760.
- (33) Piazza, Z. A.; Hu, H. S.; Li, W. L.; Zhao, Y. F.; Li, J.; Wang, L. S. Planar Hexagonal B₃₆ as a Potential Basis for Extended Single-Atom Layer Boron Sheets. *Nat. Commun.* **2014**, *5* (1), 3113.
- (34) Mannix, A. J.; Zhou, X. F.; Kiraly, B.; Wood, J. D.; Alducin, D.; Myers, B. D.; Liu, X.; Fisher, B. L.; Santiago, U.; Guest, J. R.; Yacaman, M. J.; Ponce, A.; Oganov, A. R.;

- Hersam, M. C.; Guisinger, N. P. Synthesis of Borophenes: Anisotropic, Two-Dimensional Boron Polymorphs. *Science* **2015**, *350* (6267), 1513-1516.
- (35) Feng, B. J.; Zhang, J.; Zhong, Q.; Li, W. B.; Li, S.; Li, H.; Cheng, P. P.; Meng, S.; Chen, L.; Wu, K. H. Experimental Realization of Two-Dimensional Boron Sheets. *Nat. Chem.* **2016**, *8* (6), 563-568.
- (36) Sai, L. W.; Wu, X.; Gao, N.; Zhao, J. J.; King, R. B. Boron Clusters with 46, 48, and 50 Atoms: Competition among the Core-Shell, Bilayer and Quasi-Planar Structures. *Nanoscale* **2017**, *9* (37), 13905-13909.
- (37) Chen, W. J.; Ma, Y. Y.; Chen, T. T.; Ao, M. Z.; Yuan, D. F.; Chen, Q.; Tian, X. X.; Mu, Y. W.; Li, S. D.; Wang, L. S. B₄₈⁻: A Bilayer Boron Cluster. *Nanoscale* **2021**, *13* (6), 3868-3876.
- (38) Xu, Y.; Xuan, X. Y.; Yang, T. F.; Zhang, Z. H.; Li, S. D.; Guo, W. L. Quasi-Freestanding Bilayer Borophene on Ag(111). *Nano Lett.* **2022**, *22* (8), 3488-3494.
- (39) Ma, Y. Y.; Zhao, X. Y.; Zan, W. Y.; Mu, Y. W.; Zhang, Z. H.; Li, S. D. Prediction of Freestanding Semiconducting Bilayer Borophenes. *Nano Res.* **2022**, *15* (6), 5752-5757.
- (40) Wu, X.; Liao, R.; Liang, X. Q.; Sai, L. W.; Liu, Y.; Yang, G. C.; Zhao, J. J. Pivotal Role of the B₁₂-Core in the Structural Evolution of B₅₂-B₆₄ Clusters. *Nanoscale* **2023**, *15* (24), 10430-10436.
- (41) Chen, J. H.; Liao, R.; Sai, L. W.; Zhao, J. J.; Wu, X. B₆₃: The Most Stable Bilayer Structure with Dual Aromaticity. *J. Phys. Chem. Lett.* **2024**, *15* (15), 4167-4174.
- (42) Choi, H. W.; Zhang, Y. Y.; Kahraman, D.; Xu, C. Q.; Li, J.; Wang, L. S. Boron

- Buckminsterfullerene. *ChemRxiv* **2024**. DOI:10.26434/chemrxiv-2024-2xnxl This content is a preprint and has not been peer-reviewed.
- (43) Adamo, C.; Barone, V. Toward Reliable Density Functional Methods without Adjustable Parameters: The PBE0 Model. *J. Chem. Phys.* **1999**, *110* (13), 6158-6170.
- (44) Tao, J.; Perdew, J. P.; Staroverov, V. N.; Scuseria, G. E. Climbing the Density Functional Ladder: Nonempirical Meta–Generalized Gradient Approximation Designed for Molecules and Solids. *Phys. Rev. Lett.* **2003**, *91* (14), 146401.
- (45) Krishnan, R.; Binkley, J. S.; Seeger, R.; Pople, J. A. Self Consistent Molecular Orbital Methods. Xx. A Basis Set for Correlated Wave Functions. *J. Chem. Phys.* **1980**, 72 (1), 650-654.
- (46) Grimme, S.; Ehrlich, S.; Goerigk, L. Effect of the Damping Function in Dispersion Corrected Density Functional Theory. *J. Comput. Chem.* **2011**, *32* (7), 1456-1465.
- (47) Grimme, S.; Antony, J.; Ehrlich, S.; Krieg, H. A Consistent and Accurate *Ab Initio* Parametrization of Density Functional Dispersion Correction (DFT-D) for the 94 Elements H-Pu. *J. Chem. Phys.* **2010**, *132* (15), 154104.
- (48) Frisch, M. J.; Trucks, G. W.; Schlegel, H. B.; Scuseria, G. E.; Robb, M. A.; Cheeseman, J. R.; Scalmani, G.; Barone, V.; Petersson, G. A.; Nakatsuji, H. Gaussian 16, revision C.01, 2016.
- (49) Neese, F. The Orca Program System. Wiley Interdiscip. Rev.: Comput. Mol. Sci. **2012**, 2 (1), 73-78.
- (50) Delley, B. From Molecules to Solids with the Dmol³ Approach. *J. Chem. Phys.* **2000**, *113* (18), 7756-7764.

- (51) Nosé, S. A Molecular Dynamics Method for Simulations in the Canonical Ensemble. *Mol. Phys.* **1984**, *52* (2), 255-268.
- (52) Windiks, R.; Delley, B. Massive Thermostatting in Isothermal Density Functional Molecular Dynamics Simulations. *J. Chem. Phys.* **2003**, *119* (5), 2481-2487.
- (53) Zubarev, D. Y.; Boldyrev, A. I. Developing Paradigms of Chemical Bonding: Adaptive Natural Density Partitioning. *Phys. Chem. Chem. Phys.* **2008**, *10* (34), 5207-5217.
- (54) Chen, Z. F.; Wannere, C. S.; Corminboeuf, C.; Puchta, P.; Schleyer, P. v. R. Nucleus-Independent Chemical Shifts (NICS) as an Aromaticity Criterion. *Chem. Rev.* **2005**, *105* (10), 3842-3888.
- (55) Lu, T.; Chen, F. W. Multiwfn: A Multifunctional Wavefunction Analyzer. *J. Comput. Chem.* **2012**, *33* (5), 580-592.
- (56) Humphrey, W.; Dalke, A.; Schulten, K. VMD: Visual Molecular Dynamics. *J. Mol. Graph.* **1996**, *14* (1), 33-38.
- (57) Liu, X. L.; Li, Q. C.; Ruan, Q. Y.; Rahn, M. S.; Yakobson, B. I.; Hersam, M. C. Borophene Synthesis Beyond the Single-Atomic-Layer Limit. *Nat. Mater.* **2022**, *21* (1), 35-40.
- (58) Boustani, I. Systematic Ab Initio Investigation of Bare Boron Clusters: Mdetermination of the Geometryand Electronic Structures of B_n (n=2-14). *Phys. Rev.* B **1997**, 55 (24), 16426.
- (59) Quandt, A.; Boustani, I. Boron Nanotubes. *ChemPhysChem* **2005**, *6* (10), 2001-2008.

- (60) Szwacki, N. G.; Sadrzadeh, A.; Yakobson, B. I. B₈₀ Fullerene: An *Ab Initio* Prediction of Geometry, Stability, and Electronic Structure. *Phys. Rev. Lett.* **2008**, *100* (15), 166804.
- (61) Wang, X. Q. Structural and Electronic Stability of a Volleyball-Shaped B₈₀ Fullerene. *Phys. Rev. B* **2010**, *82* (15), 153409.

Table of Contents Graphic

The existence of the bilayer B₈₀ structure is supported by experimental photoelectron spectroscopy.

